(Preprint) AAS 23-202

RELATIVE MOTION ON HIGHLY-ECCENTRIC ATMOSPHERIC ENTRY TRAJECTORIES

Samuel W. Albert* **and Hanspeter Schaub†**

Relative motion models provide a method of directly describing the position and velocity of a deputy spacecraft with respect to a chief spacecraft. Common approaches such as the Clohessy-Wiltshire equations describe relative motion in a rotating orbit frame aligned with the radial position vector of the chief, and intuitive solutions exist in this frame for circular or near-circular chief orbits. However, as eccentricity of the chief orbit increases, the along-track and velocity directions become less aligned and the orbit frame becomes less intuitive. This work revisits several key relative motion descriptions in the orbit frame and reformulates them to describe motion in the velocity frame, which is shown to be an intuitive description of motion about a highly-eccentric chief. These models are combined with the extended Allen-Eggers equations into a procedure for analytically estimating the offset in landing location for formation flying on an atmospheric entry trajectory. Three representative examples are given and compared with simulation, and range offset predictions are within 6% of total chief range in all cases.

INTRODUCTION

In studies of spacecraft formation flying it is common to represent the relevant dynamics using relative motion models centered on one spacecraft, with this central spacecraft labelled chief and all others labelled deputy.[1] These models could take the form of exact or linearized relative equations of motion (EOMs), which may admit analytical solutions, and a wide variety of solutions have been studied.[2] Such relative motion models provide a degree of analytical insight, reduce the computational complexity for simulation, and supply a dynamics representation more amenable to onboard control and estimation methods. Notably, the choice of state representation (Cartesian coordinate frame, relative orbit elements, etc.) has a significant impact on the utility of these models.[3]

Existing formation flying literature is primarily concerned with motion about circular or slightly-eccentric elliptical orbits, such as the well-known works by Hill,[4] Clohessy and Wiltshire,[5] and Tschauner and Hempel.[6] In contrast, relative motion about highly-eccentric elliptical or hyperbolic chief orbits has received little dedicated attention. Carter presents a state transition matrix (STM) applicable for Keplerian orbits with any eccentricity in terms of Cartesian coordinates in a rotating frame with true anomaly as the independent variable,[7] and a time-explicit STM is given by Dang.[8] A direct solution of the STM for any non-parabolic Keplerian orbit is given by Reynolds in terms of inertial states.[9] Dang and Zhang present linearized relative equations of motion in terms of orbit

*PhD Candidate, Ann and H.J. Smead Department of Aerospace Engineering Sciences, University of Colorado Boulder, 431 UCB, Colorado Center for Astrodynamics Research, Boulder, CO 80309. AIAA Student Member.

†Professor and Department Chair, Schaden Leadership Chair, Ann and H.J. Smead Department of Aerospace Engineering Sciences, University of Colorado, Boulder, 431 UCB, Colorado Center for Astrodynamics Research, Boulder, CO, 80309. AAS Fellow, AIAA Fellow.

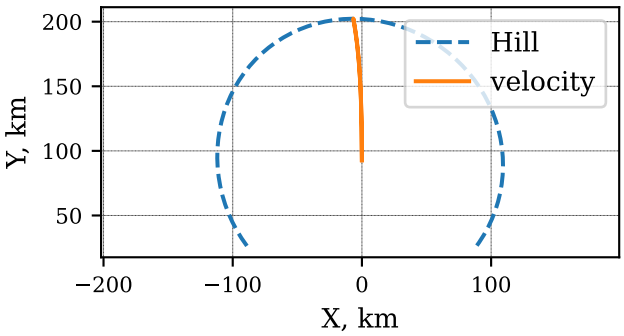

Figure 1: Relative motion about hyperbolic chief shown in Hill and velocity frame components

element differences that are valid about a hyperbolic orbit;[10] the work by Willis *et. al* gives a second-order solution in terms of time and true anomaly of the chief,[11] and Melton shows that this model holds true for hyperbolic orbits.[12] While the aforementioned approaches provide accurate models of relative motion about a highly-eccentric chief, they do not necessarily present an intuitive representation in the way that the Clohessy-Wiltshire-Hill equations do in a Cartesian rotating frame for motion about a circular chief. This is because all prior work expresses the Cartesian relative motion coordinates in the rotating orbit (or Hill) frame of the chief. This frame is not as convenient for highly-eccentric chief orbits, as even the simplest formation, the lead-follower formation in which there is only a difference in true anomaly, results in a two-dimensional trajectory in the orbit frame. The relative motion in a lead-follower formation is primarily in the velocity direction, which is not along an orbit frame unit vector for non-circular orbits. This is illustrated in Fig. 1, which shows relative motion for a lead-follower formation about a hyperbolic chief in both the Hill and velocity frames, where the y-axis of the latter is defined as the velocity direction of the chief. This paper explores what the relative motion trajectory solution is if expressed in the chief velocity frame rather than the orbit frame. This velocity frame is also of interest for entry, descent and landing applications in which atmospheric drag is purely in the anti-velocity direction.

The contributions of this work are an exploration of relative motion models in the velocity frame and the application of these models to approximate motion about a hyperbolic atmospheric entry trajectory. The relative equations of motion in the velocity frame are presented, the linearized approximation is developed, and the non-dimensional form is also provided. In addition, descriptions of velocity frame relative motion in terms of orbit element differences are derived for both elliptical and hyperbolic chief orbits. Several numerical examples demonstrate these Keplerian relative motion models. Relative motion during atmospheric flight is also considered by linearizing the Allen-Eggers solution for ballistic entry.[13] The Keplerian and atmospheric flight models are then combined to create a model of relative motion about an entry vehicle, and the approximate models are validated against numerical propagation of the full dynamics for several representative example scenarios. Relative motion models as described above would benefit an analyst designing trajectories for multiple co-delivered entry vehicles for applications such as a planetary probe network[14] or probe delivery by a carrier spacecraft on an entry trajectory,[15] as well as for multiple independently-targetable reentry vehicles[16] These models also could be incorporated into onboard guidance, navigation, and control algorithms.

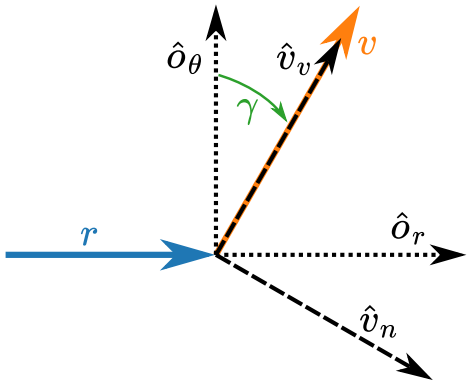

Figure 2: Hill and velocity frames

KEPLERIAN MOTION IN THE VELOCITY FRAME

Reference Frame Definitions

Let $\mathcal{N} : \{\hat{\boldsymbol{n}}_1, \hat{\boldsymbol{n}}_2, \hat{\boldsymbol{n}}_3\}$ be a generic inertial frame. The orbit frame, also known as the Hill or LVLH frame, is defined through the base vectors $\mathcal{O} : \{\hat{\boldsymbol{o}}_r, \hat{\boldsymbol{o}}_\theta, \hat{\boldsymbol{o}}_h\}$. Here $\hat{\boldsymbol{o}}_r$ is along the orbit radial direction and $\hat{\boldsymbol{o}}_h$ is along the angular momentum vector of the spacecraft $\boldsymbol{h} = \boldsymbol{r} \times \boldsymbol{v}$, where $\boldsymbol{r}$ and $\boldsymbol{v}$ are the position and inertial velocity vectors for the spacecraft, respectively. Lastly, $\hat{\boldsymbol{o}}_\theta$ completes the right-handed set and is referred to as the along-track direction. The velocity frame is defined through the base vectors $\mathcal{V} : \{\hat{\boldsymbol{v}}_n, \hat{\boldsymbol{v}}_v, \hat{\boldsymbol{v}}_h\}$ where $\hat{\boldsymbol{v}}_v$ is directed along the inertial velocity, $\hat{\boldsymbol{v}}_h = \hat{\boldsymbol{o}}_h$, and $\hat{\boldsymbol{v}}_n$ completes the right-handed set. Flight-path angle γ is defined as the angle from the along-track direction $\hat{\boldsymbol{o}}_\theta$ to the velocity direction $\hat{\boldsymbol{v}}_v$. Finally, true anomaly f is the angle between the position vector and the eccentricity vector, the latter of which is inertially fixed for Keplerian motion, such that the angular velocity between the Hill and inertial frames is $\boldsymbol{\omega}_{\mathcal{O}/\mathcal{N}} = \dot{f}\hat{\boldsymbol{o}}_h$. Figure 2 summarizes these frame definitions, where $\hat{\boldsymbol{o}}_h$ is directed out of the page.

Exact Relative Equations of Motion

The chief spacecraft position vector is defined as

$$\boldsymbol{r}_c = r_c\hat{\boldsymbol{o}}_r = x_c\hat{\boldsymbol{v}}_n + y_c\hat{\boldsymbol{v}}_v, \tag{1}$$

where r_c is the current orbit radius of the chief spacecraft, and noting that, under the assumption of Keplerian motion, the chief has no position component in the orbit-normal direction. As the orbit and velocity frame only differ by a rotation about $\hat{\boldsymbol{o}}_h$, the out-of-plane motion description is identical in both the orbit and velocity frame. This allows the following development to focus on the in-plane relative motion.

The deputy spacecraft position vector is then written in terms of the relative orbit position vector $\boldsymbol{\rho}$ as

$$\boldsymbol{r}_d = \boldsymbol{r}_c + \boldsymbol{\rho} = (x + x_c)\hat{\boldsymbol{v}}_n + (y + y_c)\hat{\boldsymbol{v}}_v + z\hat{\boldsymbol{v}}_h, \tag{2}$$

noting that here x, y, and z are defined as velocity frame components, a break from the common use of these variables as Hill frame components.

The velocity frame rotates with respect to the inertial frame with an angular velocity of $\boldsymbol{\omega}_{\mathcal{V}/\mathcal{N}}$, which expands as

$$\boldsymbol{\omega}_{\mathcal{V}/\mathcal{N}} = \boldsymbol{\omega}_{\mathcal{V}/\mathcal{O}} + \boldsymbol{\omega}_{\mathcal{O}/\mathcal{N}} = (\dot{f} - \dot{\gamma})\hat{\boldsymbol{v}}_h. \tag{3}$$

The time derivative of this vector with respect to the inertial frame, $\dot{\boldsymbol{\omega}}_{\mathcal{V}/\mathcal{N}}$, is similarly written as

$$\dot{\boldsymbol{\omega}}_{\mathcal{V}/\mathcal{N}} = \dot{\boldsymbol{\omega}}_{\mathcal{V}/\mathcal{O}} + \dot{\boldsymbol{\omega}}_{\mathcal{O}/\mathcal{N}} = (\ddot{f} - \ddot{\gamma})\hat{\boldsymbol{v}}_h. \tag{4}$$

Applying transport theorem[1] twice to Eq. (2) to find the second time derivative with respect to the inertial frame yields the following kinematic expression for the deputy spacecraft acceleration vector:

$$\begin{aligned}\ddot{\boldsymbol{r}}_d = &\left(\ddot{x} + \ddot{x}_c - 2(\dot{f} - \dot{\gamma})(\dot{y} + \dot{y}_c) - (\ddot{f} - \ddot{\gamma})(y + y_c) - (\dot{f} - \dot{\gamma})^2(x + x_c)\right)\hat{\boldsymbol{v}}_n \\ &+ \left(\ddot{y} + \ddot{y}_c + 2(\dot{f} - \dot{\gamma})(\dot{x} + \dot{x}_c) + (\ddot{f} - \ddot{\gamma})(x + x_c) - (\dot{f} - \dot{\gamma})^2(y + y_c)\right)\hat{\boldsymbol{v}}_v + \ddot{z}\hat{\boldsymbol{v}}_h.\end{aligned} \tag{5}$$

An expression for the chief spacecraft acceleration vector can be similarly derived, and in this case is equal to the Keplerian acceleration vector $-(\mu/r_c^3)\boldsymbol{r}_c$, where μ is the gravitational parameter of the central body. Equating the vector components in the resulting expression yields the following equations:

$$\ddot{x}_c - 2(\dot{f} - \dot{\gamma})\dot{y}_c - (\ddot{f} - \ddot{\gamma})y_c - (\dot{f} - \dot{\gamma})^2 x_c = -\frac{\mu}{r_c^3}x_c \tag{6a}$$

$$\ddot{y}_c + 2(\dot{f} - \dot{\gamma})\dot{x}_c + (\ddot{f} - \ddot{\gamma})x_c - (\dot{f} - \dot{\gamma})^2 y_c = -\frac{\mu}{r_c^3}y_c \tag{6b}$$

The vectors $\boldsymbol{\omega}_{\mathcal{V}/\mathcal{N}}$ and $\dot{\boldsymbol{\omega}}_{\mathcal{V}/\mathcal{N}}$ are conveniently expressed as:[1]

$$\boldsymbol{\omega}_{\mathcal{V}/\mathcal{N}} = (\dot{f} - \dot{\gamma})\hat{\boldsymbol{v}}_h = \frac{\alpha}{\zeta}\dot{f}\hat{\boldsymbol{v}}_h, \tag{7}$$

$$\dot{\boldsymbol{\omega}}_{\mathcal{V}/\mathcal{N}} = (\ddot{f} - \ddot{\gamma})\hat{\boldsymbol{v}}_h = \left(\frac{\alpha}{\zeta}\ddot{f} - \frac{e\left(e^2 - 1\right)\sin f}{\zeta^2}\dot{f}^2\right)\hat{\boldsymbol{v}}_h, \tag{8}$$

where the dimensionless quantities α and ζ are defined for ease of notation:

$$\alpha = (e\cos f + 1), \tag{9}$$

$$\zeta = (e^2 + 2e\cos f + 1). \tag{10}$$

The chief orbit angular momentum magnitude h is constant for Keplerian motion, and setting its time derivative equal to zero yields an expression for true anomaly acceleration:[1]

$$h = r_c^2\dot{f} \tag{11}$$

$$\dot{h} = 0 = 2r_c\dot{r}_c\dot{f} + r_c^2\ddot{f} \tag{12}$$

Finally, the acceleration acting on the deputy spacecraft is written as the sum of Keplerian acceleration plus an arbitrary perturbing acceleration vector $\boldsymbol{u} = u_x\hat{\boldsymbol{v}}_n + u_y\hat{\boldsymbol{v}}_v + u_z\hat{\boldsymbol{v}}_h$,

$$\ddot{\boldsymbol{r}}_d = -\frac{\mu}{r_d^3}\boldsymbol{r}_d + \boldsymbol{u}, \tag{13}$$

where $r_d = \sqrt{(x+x_c)^2 + (y+y_c)^2 + z_c^2}$ is the orbit radius of the deputy spacecraft.

Substituting Eq. (6)–(8) and (12) into Eq. (5) gives a kinematic expression for acceleration of the deputy spacecraft; equating this with the kinetic acceleration defined in Eq. (13) and simplifying yields the exact nonlinear relative equations of motion in terms of velocity frame components:

$$\ddot{x} + \dot{f}\frac{\alpha}{\zeta}\left[y\left(2\frac{\dot{r}_c}{r_c} - \frac{\dot{f}e(1-e^2)\sin f}{\alpha\zeta}\right) - 2\dot{y} - x\frac{\dot{f}\alpha}{\zeta}\right] - \frac{\mu x_c}{r_c^3} = -\frac{\mu}{r_d^3}(x_c + x) + u_x \tag{14a}$$

$$\ddot{y} - \dot{f}\frac{\alpha}{\zeta}\left[x\left(2\frac{\dot{r}_c}{r_c} - \frac{\dot{f}e(1-e^2)\sin f}{\alpha\zeta}\right) - 2\dot{x} + y\frac{\dot{f}\alpha}{\zeta}\right] - \frac{\mu y_c}{r_c^3} = -\frac{\mu}{r_d^3}(y_c + y) + u_y \tag{14b}$$

$$\ddot{z} = -\frac{\mu}{r_d^3}z + u_z \tag{14c}$$

Note that the flight-path angle of the chief spacecraft is written as

$$\tan\gamma = \frac{e\sin f}{1 + e\cos f} = \frac{e\sin f}{\alpha}. \tag{15}$$

Therefore, Eqs. (14a) and (14b) can also be written as:

$$\ddot{x} + \dot{f}\frac{\alpha}{\zeta}\left[y\left(2\frac{\dot{r}_c}{r_c} - \frac{\dot{f}(1-e^2)}{\zeta}\tan\gamma\right) - 2\dot{y} - x\frac{\dot{f}\alpha}{\zeta}\right] - \frac{\mu x_c}{r_c^3} = -\frac{\mu}{r_d^3}(x_c + x) + u_x \tag{16a}$$

$$\ddot{y} - \dot{f}\frac{\alpha}{\zeta}\left[x\left(2\frac{\dot{r}_c}{r_c} - \frac{\dot{f}(1-e^2)}{\zeta}\tan\gamma\right) - 2\dot{x} + y\frac{\dot{f}\alpha}{\zeta}\right] - \frac{\mu y_c}{r_c^3} = -\frac{\mu}{r_d^3}(y_c + y) + u_y \tag{16b}$$

It is worth briefly noting how the relative equations of motion are correctly initialized for propagation. A typical scenario is that the position and inertial velocity vectors of the chief and deputy spacecraft are known at the initial time, and the relative state must be computed. The relative position vector, $\boldsymbol{\rho}$, is computed according to Eq. (2) and rotated into the velocity frame, providing initial values for x, y, and z. To complete the full state, relative velocity components $\dot{x}$, $\dot{y}$, and $\dot{z}$ are also required, but these comprise a vector defined as the time derivative of the relative position as seen by the velocity frame. Thus, transport theorem must be applied as shown in Eq. (17),

$$^{\mathcal{V}}\begin{bmatrix}\dot{x}\\ \dot{y}\\ \dot{z}\end{bmatrix} = \frac{^{\mathcal{V}}\mathrm{d}}{\mathrm{d}t}\boldsymbol{\rho} = \dot{\boldsymbol{\rho}} - \boldsymbol{\omega}_{\mathcal{V}/\mathcal{N}} \times \boldsymbol{\rho}, \tag{17}$$

where $\dot{\boldsymbol{\rho}} = \dot{\boldsymbol{r}}_d - \dot{\boldsymbol{r}}_c$ is the difference between the inertial velocities of the deputy and chief spacecraft, and where the result is rotated into the velocity frame.

Linearized Relative Equations of Motion

In order to linearize Eqs. (14a)–(14c), assume that the distance between the chief and deputy spacecraft is small compared to the chief orbit radius, $(x, y, z) \ll r_c$. By taking a first-order Taylor series expansion about $x = y = z = 0$, r_d is approximated as

$$\frac{\mu}{r_d^3} \approx \frac{\mu}{r_c^3}(1 - 3\kappa) \tag{18}$$

where

$$\kappa = \frac{x_c x + y_c y}{r_c^2}. \tag{19}$$

Substituting Eq. (18) into the vector expression on the right-hand side of Eq. (13) and neglecting terms that are quadratic in terms of x, y, or z results in a further simplification:

$$-\frac{\mu}{r_d^3}{}^{\mathcal{V}}\begin{bmatrix} x + x_c \\ y + y_c \\ z \end{bmatrix} \approx -\frac{\mu}{r_c^3}{}^{\mathcal{V}}\begin{bmatrix} x + x_c - 3\kappa x_c \\ y + y_c - 3\kappa y_c \\ z \end{bmatrix} \tag{20}$$

Additionally, note that μ/r_c^3 can be expressed as the following identities:[1]

$$\frac{\mu}{r_c^3} = \frac{r_c}{p}\dot{f}^2 = \frac{\dot{f}^2}{\alpha}. \tag{21}$$

Substituting Eqs. (20) and (21) into Eqs. (14a)–(14c) gives the linearized relative equations of motion in terms of velocity frame components:

$$\ddot{x} + \dot{f}\frac{\alpha}{\zeta}\left[y\left(2\frac{\dot{r}_c}{r_c} - \frac{\dot{f}e(1-e^2)\sin f}{\alpha\zeta}\right) - 2\dot{y} - x\frac{\dot{f}\alpha}{\zeta}\right] + \frac{\dot{f}^2}{\alpha}(x - 3\kappa x_c) = u_x \tag{22a}$$

$$\ddot{y} - \dot{f}\frac{\alpha}{\zeta}\left[x\left(2\frac{\dot{r}_c}{r_c} - \frac{\dot{f}e(1-e^2)\sin f}{\alpha\zeta}\right) - 2\dot{x} + y\frac{\dot{f}\alpha}{\zeta}\right] + \frac{\dot{f}^2}{\alpha}(y - 3\kappa y_c) = u_y \tag{22b}$$

$$\ddot{z} + \frac{\dot{f}^2}{\alpha}z = u_z \tag{22c}$$

Non-Dimensional Relative Equations of Motion

In the case of relative motion in the Hill frame, the linearized equations of motion take on an elegant form when non-dimensionalized by the chief orbit radius r_c and differentiated with respect to the chief orbit true anomaly f instead of time.[1] These are known as the Tschauner-Hempel equations,[6] and a variety of solution approaches exist in the literature.[7] For completeness, the equivalent non-dimensional forms of the linearized relative EOMs in terms of velocity frame components are presented here.

Define the non-dimensional relative orbit coordinates (u, v, w) as

$$u = \frac{x}{r_c} \qquad v = \frac{y}{r_c} \qquad w = \frac{z}{r_c} \tag{23}$$

Unlike the Tschauner-Hempel equations in the Hill frame, the velocity frame equations require similarly defining non-dimensional coordinates for the chief spacecraft:

$$u_c = \frac{x_c}{r_c} \qquad v_c = \frac{y_c}{r_c} \qquad w_c = \frac{z_c}{r_c} \tag{24}$$

Denote the derivative with respect to chief orbit true anomaly as

$$()' \equiv \frac{\mathrm{d}()}{\mathrm{d}f} \tag{25}$$

The following identities relate time derivatives of (x, y, z) to derivatives of (u, v, z) with respect to true anomaly:[1]

$$\frac{\dot{x}}{r_c} = u'\dot{f} + u\frac{\dot{r}_c}{r_c} \qquad \frac{\ddot{x}}{r_c} = u''\dot{f}^2 + u\dot{f}^2\left(1 - \frac{r_c}{p}\right) \tag{26a}$$

$$\frac{\dot{y}}{r_c} = v'\dot{f} + v\frac{\dot{r}_c}{r_c} \qquad \frac{\ddot{y}}{r_c} = v''\dot{f}^2 + v\dot{f}^2\left(1 - \frac{r_c}{p}\right) \tag{26b}$$

$$\frac{\dot{z}}{r_c} = w'\dot{f} + w\frac{\dot{r}_c}{r_c} \qquad \frac{\ddot{z}}{r_c} = w''\dot{f}^2 + w\dot{f}^2\left(1 - \frac{r_c}{p}\right) \tag{26c}$$

Dividing Eq. (22) by r_c and substituting Eq. (26) gives the following non-dimensional linearized relative equations of motion in terms of velocity frame components:

$$u'' + \left[1 - \frac{\alpha^2}{\zeta^2} - 3\frac{r_c}{p}u_c^2\right]u - 2\frac{\alpha}{\zeta}v' - \left[\frac{e(1-e^2)\sin f}{\zeta^2} + 3\frac{r_c}{p}u_c v_c\right]v = \frac{u_x}{r_c\dot{f}^2} \tag{27a}$$

$$v'' + \left[1 - \frac{\alpha^2}{\zeta^2} - 3\frac{r_c}{p}v_c^2\right]v + 2\frac{\alpha}{\zeta}u' + \left[\frac{e(1-e^2)\sin f}{\zeta^2} - 3\frac{r_c}{p}u_c v_c\right]u = \frac{u_y}{r_c\dot{f}^2} \tag{27b}$$

$$w'' + w = \frac{u_z}{r_c\dot{f}^2} \tag{27c}$$

Relative Orbit Element Description

A disadvantage of the relative equations of motion discussed thus far is that, for a general orbit, describing the relative motion requires solving the differential equations. As an alternative approach, a direct mapping between orbit element differences and the Cartesian relative position vector $\boldsymbol{\rho}$ would provide analytical insight into the relative orbit geometry. This is provided in Ref. 17 in terms of Hill frame components. An equivalent mapping between orbit element differences and velocity frame components can be found by simply pre-multiplying that result by the direction cosine matrix (DCM) relating the two frames, ${}^{\mathcal{V}}\boldsymbol{\rho} = [VO]{}^{\mathcal{O}}\boldsymbol{\rho}$, where [VO] is:[1]

$$[VO] = \begin{bmatrix} \frac{\alpha}{\sqrt{\zeta}} & -\frac{e\sin f}{\sqrt{\zeta}} & 0 \\ \frac{e\sin f}{\sqrt{\zeta}} & \frac{\alpha}{\sqrt{\zeta}} & 0 \\ 0 & 0 & 1 \end{bmatrix} \tag{28}$$

For completeness, a brief derivation of the equations relating orbit element differences and Cartesian velocity frame position components is given here, closely following sections 14.4.1 and 14.6.1 of Ref. 1.

Define the orbit element vector as $\boldsymbol{oe} = (a, e, i, \Omega, \omega, M)^T$, consisting of semi-major axis, eccentricity, inclination, right ascension of the ascending node, argument of periapsis, and mean anomaly, respectively. The orbit element difference vector is then defined as deputy orbit element vector minus the chief orbit element vector,

$$\delta\boldsymbol{oe} = \boldsymbol{oe}_d - \boldsymbol{oe}_c = (\delta a, \delta e, \delta i, \delta\Omega, \delta\omega, \delta M)^T \tag{29}$$

In addition to the Hill frame of the chief spacecraft $\mathcal{O}$, define $\mathcal{D}$ as the Hill frame of the deputy spacecraft. Thus, ${}^{\mathcal{D}}\boldsymbol{r}_d = {}^{\mathcal{D}}(r_d, 0, 0)^T$, and recall that ${}^{\mathcal{O}}\boldsymbol{r}_d = {}^{\mathcal{O}}(x + x_c, y + y_c, z)^T$. The deputy

position vector is mapped from the deputy Hill frame to the chief velocity frame via the inertial frame as

$$^{\mathcal{V}}\boldsymbol{r}_d = [VO][ON][ND]^{\mathcal{D}}\boldsymbol{r}_d \tag{30}$$

As before, assume that the distance between deputy and chief is much less than the chief radius, $(x, y, z) \ll r_c$. Taking the first variations of $[ND]$ and r_d about the chief spacecraft gives the following first-order approximations[1]

$$[ND] \approx [NO] + [\delta NO] \tag{31}$$

$$r_d \approx r_c + \delta r \tag{32}$$

Substituting these approximations into Eq. (30) yields

$$^{\mathcal{V}}\boldsymbol{r}_d = [VO]\left(\mathbb{I}_3 + [ON][\delta NO]\right)\begin{bmatrix} r_c + \delta r \\ 0 \\ 0 \end{bmatrix} \tag{33}$$

where $\mathbb{I}_3$ is the 3x3 identity matrix.

Note that the deputy position vector can be written as

$$^{\mathcal{V}}\boldsymbol{r}_d = {}^{\mathcal{V}}\boldsymbol{\rho} + [VO]\,{}^{\mathcal{O}}\begin{bmatrix} r_c \\ 0 \\ 0 \end{bmatrix} \tag{34}$$

Substituting Eq. (34) into Eq. (33), dropping the second-order terms associated with $[\delta NO](\delta r, 0, 0)^T$, and simplifying, the following expression is obtained

$$^{\mathcal{V}}\boldsymbol{\rho} = [VO]\left({}^{\mathcal{O}}\begin{bmatrix} \delta r \\ 0 \\ 0 \end{bmatrix} + [ON][\delta NO]\,{}^{\mathcal{O}}\begin{bmatrix} r_c \\ 0 \\ 0 \end{bmatrix}\right) \tag{35}$$

Ref. 1 shows that the parenthetical in the right-hand side of Eq. (35) is equivalent to $^{\mathcal{O}}\boldsymbol{\rho}$ and can be expressed as:

$$^{\mathcal{O}}\boldsymbol{\rho} = \begin{bmatrix} \delta r \\ r(\delta\theta + \cos i\delta\Omega) \\ r(\sin\theta\delta i - \cos\theta\sin i\delta\Omega \end{bmatrix} \tag{36}$$

While Eq. (36) provides a linearized mapping between orbit element differences and Cartesian relative position, it is inconvenient to rely on $\delta\theta$ because this varies throughout the orbit for non-circular chief spacecraft. Thus, the following developments reformulate this expression to instead rely on difference in mean anomaly M (or, in the case of a hyperbolic cheif, mean hyperbolic anomaly N), which will remain constant if $\delta a = 0$ for Keplerian motion.[1]

The variation of orbit radius is expressed as[1]

$$\delta r = \frac{r}{a}\delta a + \frac{V_r}{V_t}r\delta\theta - \frac{r}{p}(2aq_1 + r\cos\theta)\delta q_1 - \frac{r}{p}(2aq_2 + r\sin\theta)\delta q_2, \tag{37}$$

where

$$V_r = \dot{r} = \frac{h}{p}(q_1 \sin\theta - q_2 \cos\theta) \tag{38a}$$

$$V_t = r\dot{\theta} = \frac{h}{p}(1 + q_1 \cos\theta + q_2 \sin\theta), \tag{38b}$$

$$q_1 = e\cos\omega \tag{39a}$$

$$q_2 = e\sin\omega, \tag{39b}$$

and

$$\theta = f + \omega. \tag{40}$$

Note also the orbit identities:

$$r = \frac{p}{\alpha} \tag{41}$$

$$p = a(1 - e^2) \tag{42}$$

Taking the first-order variations of Eqs. (39) and (40) gives expressions for their corresponding orbit element differences:

$$\delta q_1 = \cos\omega\delta e - e\sin\omega\delta\omega \tag{43}$$

$$\delta q_2 = \sin\omega\delta e + e\cos\omega\delta\omega \tag{44}$$

$$\delta\theta = \delta f + \delta\omega \tag{45}$$

At this point the derivations diverge depending on whether mean anomaly M or mean hyperbolic anomaly N are used, corresponding to an elliptical or hyperbolic chief, respectively. The steps only differ slightly and are therefore shown here in parallel.

Take the definitions of mean anomalies M and N in terms of eccentric anomaly E and hyperbolic anomaly H:

$$M = E - e\sin E \tag{46a}$$

$$N = e\sinh H - H \tag{46b}$$

and take the first variations of these expressions:

$$\delta M = (1 - e\cos E)\delta E - \sin E\delta e \tag{47a}$$

$$\delta N = (e\cosh H - 1)\delta H + \delta e\sinh H \tag{47b}$$

Note the orbit identities relating E and H with f,[1]

$$\tan\frac{f}{2} = \sqrt{\frac{1+e}{1-e}}\tan\frac{E}{2} \tag{48a}$$

$$\tanh\frac{f}{2} = \sqrt{\frac{e+1}{e-1}}\tanh\frac{H}{2}, \tag{48b}$$

and take the first variations:

$$\delta E = \frac{\eta}{\alpha}\delta f - \frac{\sin f}{\alpha\eta}\delta e \tag{49a}$$

$$\delta H = \frac{\eta_h}{e+\cosh f}\delta f + \frac{\sinh f}{\eta_h(e+\cosh f)}\delta e \tag{49b}$$

where $\eta = \sqrt{1-e^2}$ and $\eta_h = \sqrt{e^2-1}$.

Additionally, note the following orbit identities:[1]

$$\sin E = \frac{\eta \sin f}{\alpha} \qquad \cos E = \frac{e+\cos f}{\alpha} \tag{50a}$$

$$\sinh H = \frac{\eta_h \sin f}{\alpha} \qquad \cosh H = \frac{e+\cos f}{\alpha} \tag{50b}$$

Substituting Eqs. (49) and (50) into Eq. (47), simplifying, and rearranging provides expressions for δf in terms of δM and δN:

$$\delta f = \frac{\alpha^2}{\eta^3}\delta M + \frac{\sin f(2+e\cos f)}{1-e^2}\delta e \tag{51a}$$

$$\delta f = \frac{\alpha^2}{\eta_h^3}\delta N - \frac{\sin f(2+e\cos f)}{e^2-1}\delta e \tag{51b}$$

$$\tag{51c}$$

Substituting the orbit identities given in Eqs. (37) – (45) and (51) into Eqs. (36), pre-multipliying by $[VO]$, and simplifying yields the desired mapping, where Eq. (52) and Eq. (53) correspond to ellitical and hyperbolic chief orbits, respectively.

$$x = \frac{(1-e^2)}{\sqrt{\zeta}}\delta a - \frac{a\left(\left(e^2+1\right)\cos f + 2e\right)}{\alpha\sqrt{\zeta}}\delta e - \frac{re\sin f}{\sqrt{\zeta}}(\delta\omega + \delta\Omega\cos i) \tag{52a}$$

$$y = \frac{re\sin f}{a\sqrt{\zeta}}\delta a + \frac{2a\sin f}{\sqrt{\zeta}}\delta e + \frac{p}{\sqrt{\zeta}}(\delta\omega + \delta\Omega\cos i) + \frac{a\sqrt{\zeta}}{\eta}\delta M \tag{52b}$$

$$z = r\left(\sin\theta\delta i - \sin i\cos\theta\delta\Omega\right) \tag{52c}$$

$$x = \frac{(1-e^2)}{\sqrt{\zeta}}\delta a - \frac{a\left(\left(e^2+1\right)\cos f + 2e\right)}{\alpha\sqrt{\zeta}}\delta e - \frac{re\sin f}{\sqrt{\zeta}}(\delta\omega + \delta\Omega\cos i) \tag{53a}$$

$$y = \frac{re\sin f}{a\sqrt{\zeta}}\delta a + \frac{2a\sin f}{\sqrt{\zeta}}\delta e + \frac{a(1-e^2)}{\sqrt{\zeta}}(\delta\omega + \delta\Omega\cos i) - \frac{a\sqrt{\zeta}}{\eta_h}\delta N \tag{53b}$$

$$z = r\left(\sin\theta\delta i - \sin i\cos\theta\delta\Omega\right) \tag{53c}$$

By sweeping chief true anomaly values through a single full revolution, the corresponding relative orbit geometry can be analytically computed according to Eq. (52). In the case of an invariant orbit, where $\delta a = 0$ and the dynamics are fully Keplerian, this describes the complete relative orbit

geometry. It is important to note that in the case of a hyperbolic chief, the equations should only be evaluated for physically-reachable values of true anomaly as defined by the range $(-f_\infty, f_\infty)$ where f_∞ is the asymptotic true anomaly:

$$\cos f_\infty = -\frac{1}{e} \tag{54}$$

Note that it is possible for α to equal 0 and cause a singularity in Eq. 53 for hyperbolic orbits if this constraint is ignored, but that this singularity is never encountered as long as the physical limitation of $-f_\infty < f < f_\infty$ is respected.

In order to fully describe the spacecraft state, velocity is also necessary, and this can be obtained by differentiating Eqs. (52) and (53) with respect to time. The only time-varying quantities appearing in these equations are true anomaly of the chief f and either difference in mean anomaly δM or difference in mean hyperbolic anomaly δN, respectively. The conservation of angular momentum of the chief spacecraft, given by Eq. (11), can be rearranged to give an expression for $\dot{f}$,

$$\dot{f} = \frac{h}{r_c^2}. \tag{55}$$

To find expressions for $\delta\dot{M}$ and $\delta\dot{N}$, begin with Kepler's equation,[1]

$$M = M_0 + n(t - t_0) \tag{56a}$$

$$N = N_0 + n(t - t_0), \tag{56b}$$

where $n = \sqrt{\mu/a^3}$ is the mean motion, and take the first variation,

$$\delta M = \delta M_0 - \frac{3}{2}\frac{\delta a}{a}(M - M_0) \tag{57a}$$

$$\delta N = \delta N_0 - \frac{3}{2}\frac{\delta a}{a}(N - N_0). \tag{57b}$$

Taking the time derivative of Eq. (57) gives the desired expressions,

$$\delta\dot{M} = \delta\dot{N} = -\frac{3}{2}\frac{\delta a}{a}n. \tag{58}$$

Eqs. (59) and (60) give the resulting mappings, for elliptical and hyperbolic chief orbits respectively, from orbit element differences to components of the time derivative of the relative position vector with respect to the velocity frame. Note that the inertial velocity of the deputy can be recovered from the relative velocity components by rearranging Eq. (17).

$$\begin{aligned}\dot{x} = {} & \frac{eh\alpha\sin f}{ar\zeta^{3/2}}\delta a + \frac{h\sin f\left[\left(e^2+1\right)\left(\zeta\alpha - e\cos f(\alpha+\zeta)\right) - 2e^2(\alpha+\zeta)\right]}{p\left(1-e^2\right)\zeta^{3/2}}\delta e \\ & - \frac{eh\left(\zeta\alpha\cos f + e\sin^2 f(\alpha+\zeta)\right)}{p\zeta^{3/2}}(\delta\omega + \delta\Omega\cos i)\end{aligned} \tag{59a}$$

$$\begin{aligned}\dot{y} = {} & \left(\frac{eh\left(\zeta\alpha\cos f + e\sin^2 f(\alpha+\zeta)\right)}{ap\zeta^{3/2}} - \frac{3n\sqrt{\zeta}}{2\eta}\right)\delta a + \frac{2h\alpha\left(\zeta\cos f + e\sin^2 f\right)}{r\left(1-e^2\right)\zeta^{3/2}}\delta e \\ & + \frac{eh\alpha\sin f}{r\zeta^{3/2}}(\delta\omega + \delta\Omega\cos i) - \frac{eh\alpha\sin f}{r\eta^3\sqrt{\zeta}}\delta M\end{aligned} \tag{59b}$$

$$\dot{z} = \frac{h}{p}(e\cos\omega + \cos\theta)\delta i + \frac{h}{p}\sin i(e\sin\omega + \sin\theta)\delta\Omega \tag{59c}$$

$$\dot{x} = \frac{eh\alpha \sin f}{ar\zeta^{3/2}}\delta a + \frac{h \sin f \left[\left(e^2+1\right)\left(\zeta\alpha - e\cos f(\alpha+\zeta)\right) - 2e^2(\alpha+\zeta)\right]}{p\left(1-e^2\right)\zeta^{3/2}}\delta e$$
$$- \frac{eh\left(\zeta\alpha\cos f + e\sin^2 f(\alpha+\zeta)\right)}{p\zeta^{3/2}}(\delta\omega + \delta\Omega\cos i) \tag{60a}$$

$$\dot{y} = \left(\frac{eh\left(\zeta\alpha\cos f + e\sin^2 f(\alpha+\zeta)\right)}{ap\zeta^{3/2}} + \frac{3n\sqrt{\zeta}}{2\eta_h}\right)\delta a + \frac{2h\alpha\left(\zeta\cos f + e\sin^2 f\right)}{r\left(1-e^2\right)\zeta^{3/2}}\delta e$$
$$+ \frac{eh\alpha\sin f}{r\zeta^{3/2}}(\delta\omega + \delta\Omega\cos i) - \frac{eh\alpha\sin f}{r\eta_h^3\sqrt{\zeta}}\delta N \tag{60b}$$

$$\dot{z} = \frac{h}{p}(e\cos\omega + \cos\theta)\delta i + \frac{h}{p}\sin i(e\sin\omega + \sin\theta)\delta\Omega \tag{60c}$$

Numerical Examples

To illustrate relative motion behavior in the velocity frame and demonstrate the equations derived above, two example scenarios are briefly shown in this subsection. The equations of motion are numerically propagated using the Runge-Kutta method of order 5(4) via the open-source scipy.integrate.solve_ivp tool,[18,19] with relative and absolute error tolerances of 1×10^{-12}, using a value of $3.986 \times 10^5\,\mathrm{km}^3/\mathrm{s}^2$ for μ.[20] Table 1 summarizes the chief orbit parameters and orbit element differences for each scenario, and Figs. 3 and 4 show the results for Scenarios A and B, respectively. In these figures "absolute" refers to separate simulation of the Keplerian dynamics, "relative" refers to propagation of the exact relative EOMs, "linaerized" refers to propagation of the linearized relative EOMs, and "oe differences" refers to sweeping through the relative orbit element equations for all relevant true anomaly values.

Scenario A is a lead-follower formation. As mentioned in the introduction, almost all of the relative motion is along the velocity direction, with only a small component along $\hat{\boldsymbol{v}}_n$. The linearization ignores this $\hat{\boldsymbol{v}}_n$ component and traverses down and back up along $\hat{\boldsymbol{v}}_v$. These results also show perfect agreement between the absolute and relative EOMs, as is expected in the absence of any approximations or non-Keplerian accelerations. Scenario B captures the behavior of a deputy spacecraft offset only in eccentricity. The lower-right plot intuitively shows how the deputy begins ahead of the chief, comes closer as the two spacecraft approach periapsis, and is behind the chief after periapsis.

APPLICATION TO ATMOSPHERIC ENTRY TRAJECTORIES

The relative motion models developed thus far assume a chief spacecraft governed only by Keplerian dynamics. In this section, these models are combined with an analytical approximation of hypersonic flight mechanics to make predictions of relative motion about atmospheric entry trajectories. The exoatmospheric portions of entry trajectories are typically either hyperbolic (in the case

Table 1: Orbital parameters for example scenarios

Scenario	a	e	i	Ω	ω	δa	δe	δi	$\delta\Omega$	$\delta\omega$	δM_0
A	$-7000\,\mathrm{km}$	1.2	0	0	0	0	0	0	0	0	0.5°
B	$-7000\,\mathrm{km}$	1.2	0	0	0	0	0.005	0	0	0	0

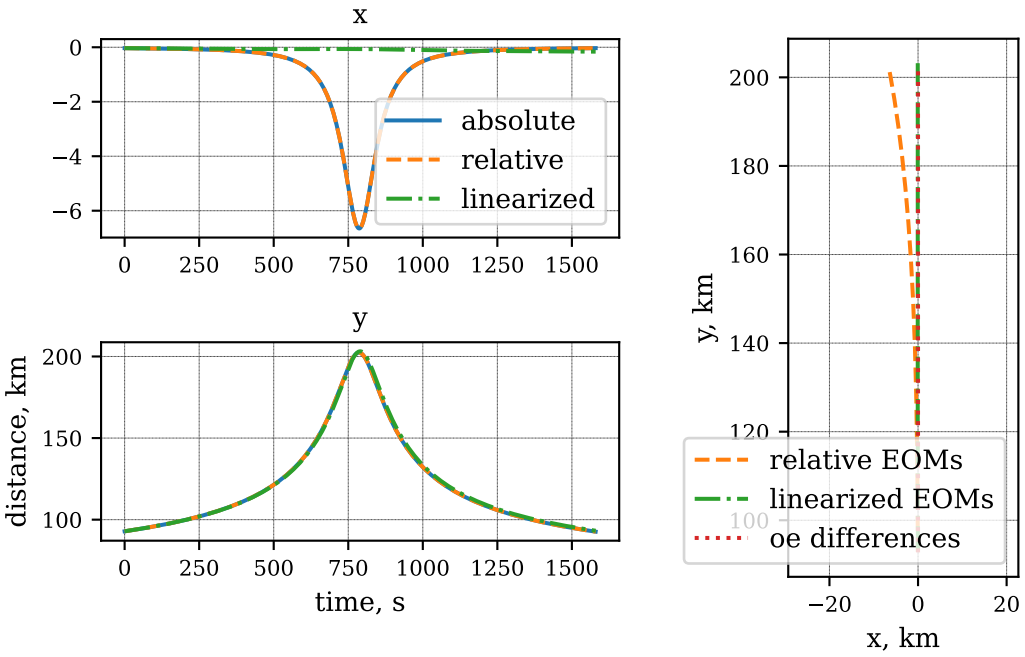

Figure 3: Relative motion for Scenario A

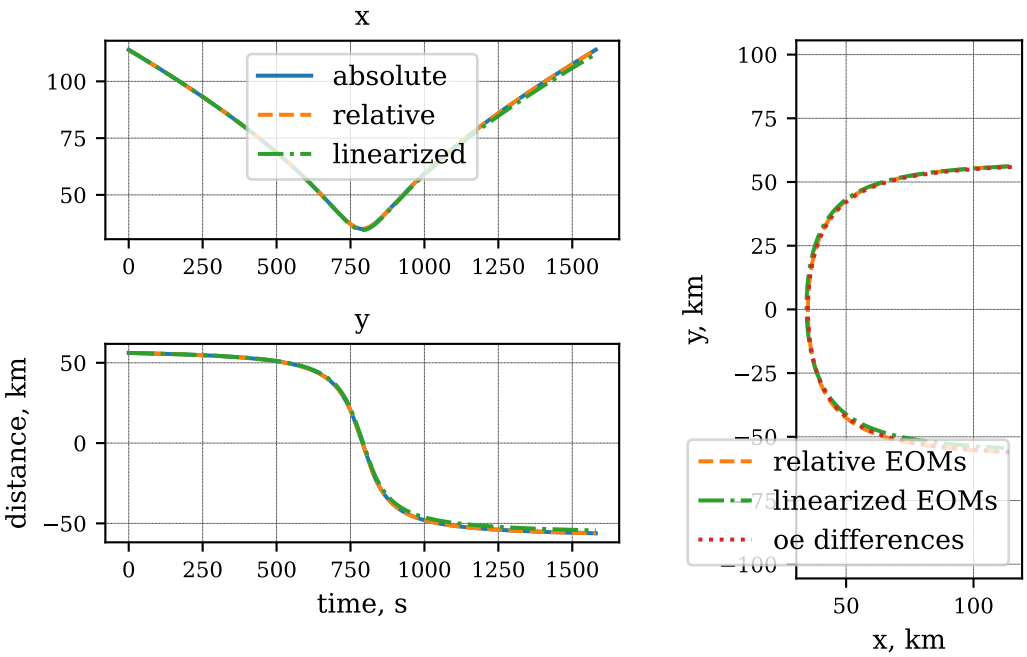

Figure 4: Relative motion for Scenario B

of sample return or planetary exploration) or highly elliptical (in the case of suborbital defense or rapid transport applications), and therefore the velocity frame descriptions of relative motion are well-suited for these applications. Relevant example missions include probe delivery by a carrier spacecraft on an entry trajectory,[14] co-delivery of a probe network,[15] or multiple independently-targetable reentry vehicles.[16]

Enhanced Allen-Eggers Equations

The Allen-Eggers equations were developed in the 1950's and provide an analytical, closed-form description of ballistic (nonlifting) entry under certain assumptions relevant to the missile applications for which they were originally derived.[13,21] Namely, these assumptions include:

- Ballistic entry, meaning a lift-to-drag ratio of $L/D = 0$
- Constant flight-path angle, $\dot{\gamma} = 0$
- Gravity is negligible compared to drag force, $D \gg g \sin\gamma$
- Zero thrust and constant mass, $T = \dot{m} = 0$
- Nonrotating planet, such that inertial and planet-relative velocity and flight-path angle are identical

Additionally, atmospheric density ρ is assumed to be an exponential function of altitude h,

$$\rho(h) = \rho_{\text{ref}} \exp\left(\frac{h_{\text{ref}} - h}{H}\right), \tag{61}$$

where ρ_{ref} and h_{ref} are reference density and altitude (typically defined at sea level), respectively, and H is atmospheric scale height. A key parameter in the resulting equations is ballistic coefficient β,

$$\beta = \frac{m}{C_D A}, \tag{62}$$

where m, C_D, and A are the mass, drag coefficient, and aerodynamic reference area of the vehicle, respectively. Ballistic coefficient can be understood as the ratio of inertial to aerodynamic forces on the vehicle, and will be treated as constant, generally a good approximation for hypersonic flight.[22] Note that throughout this section the subscript x_0 refers to the value at entry, defined as reaching the atmospheric interface altitude $h_0 = r_0 - R$, whereas the subscript x_i refers to the value at some earlier exoatmospheric initial state.

In the original development of the Allen-Eggers equations, flight-path angle is assumed to be constant at its value at entry, $\gamma^* = \gamma_0$.[13] This is a good approximation for steep entries, but for shallow entry trajectories an alternate value can improve accuracy.[23] The closed-form expression given in Ref. 24, described below, is used to compute γ^* in this study and was found to improve prediction accuracy in the examples shown later in this section. Let V_0, γ_0, and ρ_0 be the velocity, flight-path angle, and density at entry, respectively. Additionally, let $V_C = \sqrt{gR}$ be circular velocity where g is acceleration due to gravity at the surface and R is planetary radius. Then, γ^* is computed

as

$$\sin\gamma^* = \sin\gamma_0(2F^* - 1) \tag{63a}$$

$$F^* = \sqrt{1 + \frac{H}{R\tan^2\gamma_0}\left\{C\frac{V_C^2}{V_0^2} + \left(\frac{V_C^2}{V_0^2} - 1\right)\ln\left(1 - \frac{\beta\sin\gamma_0}{H\rho_0}\right)\right\}} \tag{63b}$$

$$C = \mathrm{Ei}(1) - \Gamma \approx 1.3179 \tag{63c}$$

where $\mathrm{Ei}(x)$ is the exponential integral

$$\mathrm{Ei}(x) = -\int_{-x}^{\infty} \frac{e^{-y}}{y}\mathrm{d}y \tag{64}$$

and $\Gamma \approx 0.57722$ is the Euler-Mascheroni constant.

The original Allen-Eggers equations do not include a closed-form expression for range, meaning distance along the planetary surface from the point of atmospheric entry to landing. However, Putnam and Braun develop such an expression in an extension and enhancement of the Allen-Eggers equations by directly integrating the simplified equations of motion and without making any additional assumptions.[24] Range s between the entry radius r_0 and current radius r can thus be estimated as:

$$s = \frac{\ln(r) - \ln(r_0)}{\tan\gamma^*}R \tag{65}$$

An expression for the offset in range between the chief and deputy landing locations (where $r = R$) can be derived by taking the first variation of Eq. (65) with respect to the entry radius and constant flight-path angle:

$$\delta s(r = R) = -R\left(\frac{\delta r_0}{r_0\tan\gamma^*} + \frac{\ln(R) - \ln(r_0)}{\sin^2\gamma^*}\delta\gamma^*\right) \tag{66}$$

Note that in Eq. (66) $\delta r_0 = r_d - r_c$ and $\delta\gamma^* = \gamma_d^* - \gamma_c^*$ are both computed at the moment when the chief vehicle reaches atmospheric interface, $r_c = r_0$.

Methodology

By combining the relative orbit element expressions with Eq. (66), the range offset between landing locations due to a maneuver during exoatmospheric approach can be predicted analytically. This subsection gives an overview of the step-by-step procedure combining these relative motion models.

First, define the state of the chief and deputy vehicles at an initial time prior to atmospheric entry, and compute the relative orbit elements $\delta\boldsymbol{oe}$. In this work the chief state is computed by defining a state at atmospheric interface, computing Keplerian orbital elements, then changing the mean anomaly to a value of $M = -90^\circ$ to obtain a state on that same orbit earlier in time. The Cartesian chief state is then computed and rotated into the velocity frame, and the deputy state is defined by adding a maneuver defined in the velocity frame. That is, the chief and deputy have identical position and different velocity vectors at the initial time. The deputy state is then converted to orbit elements and used to compute $\delta\boldsymbol{oe}$.

Second, the true anomaly of the chief vehicle at atmospheric interface altitude is computed via Eq. (41):

$$f_0 = \cos^{-1}\left(\frac{a(1-e^2)}{r_0 e} - \frac{1}{e}\right) \tag{67}$$

Third, the relative orbit element equations (Eqs. (52) and (59) for an elliptical chief or Eqs. (53) and (60) for a hyperbolic chief) are applied to compute the relative state of the deputy vehicle in the velocity frame at the epoch when the chief is at atmospheric entry.

Fourth, compute the radial position r, velocity magnitude V, and flight-path angle γ of both the chief and deputy. This requires converting the chief Keplerian state to inertial Cartesian vectors, as well as converting the velocity frame relative deputy state to an inertial absolute state. Fifth, compute δr_0 and $\delta\gamma^*$. Note that when evaluating Eq. (63) for the deputy the values used for γ_0, V_0, and ρ_0 are those at the time of *chief* entry, which for the general case is not identical to the state of the deputy at entry. Sixth, compute δs from Eq. (66); this is the range offset at landing predicted due to differences in entry states of the two vehicles. The predicted bearing of this offset is assumed to equal the heading angle of the chief at entry, $\psi_B = \psi_{0,c}$, where heading angle ψ is the angle between the horizontal projection of the velocity vector and a due-North vector in that same plane (e.g. a 90° heading angle is due-East).

The procedure could stop here, but tends to be more accurate with an additional step. Due to the assumptions of the Allen-Eggers relations, Eq. (66) is poor at modeling cases such as a lead-follower, where δr_0 and $\delta\gamma^*$ are nonzero at the time of chief entry but the actual range offset will be very small, due only to the rotation of the planet between chief and deputy entries. Furthermore, Allen-Eggers assumes planar motion and is therefore unable to capture range offset due to out-of-plane relative motion between the chief and deputy. Thus, the seventh and final step is to compute range offset at time of chief entry δs_0 and geometrically combine δs_0 with δs to find the final prediction for range offset on the surface, δs_f. To do so, use the latitude and longitude of the deputy at time of chief entry along with the predicted range offset magnitude and bearing to compute an offset pair of coordinates. Then, compute the range and bearing angle from the coordinates of the chief at entry to the pair of coordinates just computed; this provides the final estimate of range and bearing between the chief and deputy landing locations. For convenience, Appendix B lists the equations required for this final step.

Results

The procedure for analytically estimating range offset is applied to three ballistic entry vehicles and trajectories, chosen to serve as representative examples and to align with the examples selected in Ref. 24. The first scenario is based on the sample return capsule for the NASA Stardust mission,[25,26] which entered Earth's atmosphere on a hyperbolic return trajectory. A second scenario is constructed as a modified version of the Stardust scenario with a steeper entry flight-path angle. The third scenario is a "high ballistic coefficient vehicle on a steep, high-energy suborbital trajectory[24]"; this case is referred to as strategic and is representative of a ballistic missile re-entry trajectory.[27] The parameters for each scenario are summarized in Table 2. In every case, the radius at entry is defined as the atmospheric interface altitude $r_0 = 125\,\mathrm{km}$, with entry longitude θ_0 and latitude ϕ_0 set to 0° and an entry heading angle of $\psi_0 = 70^\circ$. The chief orbit is fully defined by the entry state, but the semi-major axis, eccentricity, and final range are also included for reference.

For each chief orbit scenario, three different deputy orbits are considered. In each case the chief is initialized with a mean anomaly of $M = -90^\circ$, the deputy is initialized at the identical position, and

Table 2: Entry trajectory chief orbit descriptions

Scenario	V_0, km/s	γ_0, deg.	β, $\mathrm{kg/m^2}$	a, km	e	s_c, km
Stardust	12.8	-8.2	60	-7554.	1.848	805.064
Steep Stardust	12.8	-15	60	-7593.	1.815	375.745
Strategic	7.2	-30	10000	6136.	0.477	213.991

the velocity vector of the deputy at the initial time is modified by a maneuver with $\Delta V = 10\,\mathrm{m/s}$. The three deputy scenarios correspond to directing this maneuver along each of the unit vectors of the velocity frame of the chief spacecraft. Thus, nine total scenarios are considered in this section.

Parameter values $R = 6378.14\,\mathrm{km}$, $g = 9.81\,\mathrm{m/s}$, $H = 8.5\,\mathrm{km}$, $\rho_{\mathrm{ref}} = 1.215\,\mathrm{kg/m^3}$, and $h_{\mathrm{ref}} = 0\,\mathrm{km}$ are assumed for the purpose of the analytical predictions.[20,28] These predictions are compared against a numerical simulation of the full three degree-of-freedom equations of motion for a vehicle subject to point-mass gravity and drag, including the effect of a rotating planet. Numerical integration is performed using the Runge-Kutta method of order 5(4) via the open-source scipy.integrate.solve_ivp tool,[18,19] with relative and absolute error tolerances of 1×10^{-12}. The simulation models density by linearly interpolating from a table output by the Earth Global Reference Atmospheric Model;[29] the data are sufficiently dense that linear interpolation is accurate despite the approximately exponential nature of density.

Figure 5 and Table 3 summarize the comparison between predicted and simulated range offset for each of the nine scenarios under consideration. Figure 5 shows the magnitude of the percent error, meaning normalized by the simulated range offset, whereas Table 3 reports the absolute values. Table 4 compares the predicted and simulated bearing of the offset between chief and deputy landing locations in each scenario, and shows that the predicted bearing was approximately correct in all cases.

Table 3: Simulated and analytically predicted range offsets, km

	$\hat{\boldsymbol{v}}_n$		$\hat{\boldsymbol{v}}_v$		$\hat{\boldsymbol{v}}_h$	
Scenario	truth	pred.	truth	pred.	truth	pred.
Stardust	287.737	334.617	58.484	81.031	13.059	12.772
Steep Stardust	69.809	78.490	14.660	16.537	12.808	12.497
Strategic	5.780	5.565	1.880	1.903	2.934	2.547

Table 4: Simulated and analytically predicted offset bearing, deg

	$\hat{\boldsymbol{v}}_n$		$\hat{\boldsymbol{v}}_v$		$\hat{\boldsymbol{v}}_h$	
Scenario	truth	pred.	truth	pred.	truth	pred.
Stardust	70.163	69.985	70.357	70.124	-18.103	-16.553
Steep Stardust	70.005	69.964	70.766	70.613	-18.945	-18.603
Strategic	70.187	70.137	72.119	71.773	-18.575	-18.321

In the cases of maneuvers along the $\hat{\boldsymbol{v}}_n$ and $\hat{\boldsymbol{v}}_v$ directions, the predictions are consistently most accurate for the strategic scenario and least accurate for the Stardust scenario. This is as expected; the steep flight-path angle and high ballistic coefficient of the strategic scenario mean the Allen-Eggers assumptions are much more accurate than in the case of Stardust, despite the higher entry

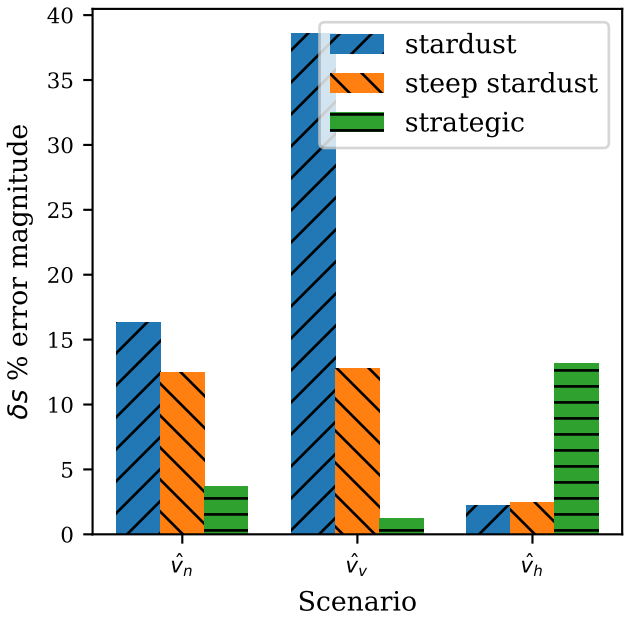

Figure 5: Absolute value of percent error of range offset error, where x-axis label denotes direction of $10\,\mathrm{m/s}$ maneuver during approach

speed of the latter. Most of the error present in the range predictions for these cases is due to the disparity between the true entry trajectories and the Allen-Eggers approximations. The cases corresponding to a maneuver along $\hat{\boldsymbol{v}}_h$ appear to present an exception to this trend based on Fig. 5, but examination of Table 3 reveals that the actual error is similarly small (within $0.5\,\mathrm{km}$) in all cases. Maneuvering along $\hat{\boldsymbol{v}}_h$ primarily serves to offset the orbital plane of the deputy. As a result, the difference in r_0, γ^*, and V_0 is negligibly small, but the deputy enters at a different location and with a different heading angle. Thus, in the $\hat{\boldsymbol{v}}_h$ cases almost all of the final range offset is due to existing offset at entry, as accounted for by step 7 of the prediction procedure. Finally, note that while the percent error values are relatively high in some cases, the errors are small compared to the total range covered by the chief (s_c in Table 2): less than 6% in all cases.

CONCLUSIONS

Describing relative motion in terms of velocity frame components can be an intuitive model for motion about highly-eccentric chief spacecraft, and provides a complementary alternative to traditional descriptions in the Hill frame. The equations of motion and orbit element difference equations developed in this work give a direct approach that could be appropriate for onboard use, such as within a navigation filter or for the design of reference trajectories. Results for several simple scenarios about a hyperbolic chief show good agreement between the linearized and exact solutions and develop a more intuitive understanding of the types of relative motion possible about flyby or atmospheric entry trajectories. The procedure developed in this work for analytically predicting the offset in final range for an atmospheric entry trajectory extends the range of application of these relative motion models to include steep ballistic entry vehicles, such as planetary probes. This method would enable rapid onboard estimation of the impact of a maneuver during approach on the

entry, descent, and landing profile of ballistic probes.

ACKNOWLEDGMENT

S. W. Albert thanks Zachary Putnam for helpful discussions regarding the enhanced Allen-Eggers equations. This work was supported by a NASA Space Technology Research Fellowship.

APPENDIX A: AUXILIARY VARIABLE DEFINITIONS

$$\zeta = (e^2 + 2e\cos f + 1) \tag{68}$$

$$\alpha = (e\cos f + 1) \tag{69}$$

$$\kappa = \frac{x_c x + y_c y}{r_c^2}, \tag{70}$$

$$\eta = \sqrt{1 - e^2} \tag{71}$$

$$\eta_h = \sqrt{e^2 - 1} \tag{72}$$

APPENDIX B: USEFUL COORDINATE RELATIONSHIPS

Let θ and ϕ be longitude and latitude, respectively, and model the central body as a perfect sphere for the purpose of these equations. The range (great circle distance) between points (θ_1, ϕ_1) and (θ_2, ϕ_2) is

$$d = R\cos^{-1}\left(\sin\phi_1\sin\phi_2 + \cos\phi_1\cos\phi_2\cos(|\theta_2 - \theta_1|)\right) \tag{73}$$

and the bearing between them (e.g. the heading angle of the great circle arc connecting the points) is

$$\psi_B = \tan^{-1}\left(\frac{\cos\phi_2\sin(\theta_2 - \theta_1)}{\cos\phi_1\sin\phi_2 - \sin\phi_1\cos\phi_2\cos(\theta_2 - \theta_1)}\right) \tag{74}$$

In the case where the coordinates of point 1 are known, along with the great circle distance and bearing between it and point 2, the coordinates of the second point can be computed as

$$\theta_2 = \theta_1 + \tan^{-1}\left(\frac{\sin\psi_B\sin(d/R)\cos\phi_1}{\cos(d/R) - \sin\phi_1\sin\phi_2}\right) \tag{75a}$$

$$\phi_2 = \sin^{-1}\left(\sin\phi_1\cos(d/R) + \cos\phi_1\sin(d/R)\cos\psi_B\right) \tag{75b}$$

REFERENCES

[1] H. Schaub and J. L. Junkins, *Analytical Mechanics of Space Systems*, pp. 536–538, 775–780, 873–876. AIAA, fourth ed., 2018.

[2] J. Sullivan, S. Grimberg, and S. D'Amico, "Comprehensive Survey and Assessment of Spacecraft Relative Motion Dynamics Models," *Journal of Guidance, Control, and Dynamics*, Vol. 40, No. 8, 2017, pp. 1837–1859, 10.2514/1.G002309.

[3] E. R. Burnett, *Novel Dynamics and Control Formulations for Multi-Spacecraft Formation Flying, Rendezvous, and Proximity Operations*. PhD thesis, University of Colorado Boulder, 2021.

[4] G. W. Hill, "Researches in the Lunar Theory," *American Journal of Mathematics*, Vol. 1, No. 1, 1878, pp. 5–26.

[5] W. H. Clohessy and R. S. Wiltshire, "Terminal Guidance System for Satellite Rendezvous," *Journal of the Aerospace Sciences*, Vol. 27, No. 9, 1960, pp. 653–658, 10.2514/8.8704.

[6] J. Tschauner and P. Hempel, "Rendezvous zu einem in Elliptischer Bahn Umlaufenden Ziel," *Acta Astronautica*, Vol. 11, No. 2, 1965, pp. 104–109.

[7] T. E. Carter, "State Transition Matrices for Terminal Rendezvous Studies: Brief Survey and New Example," *Journal of Guidance, Control, and Dynamics*, Vol. 21, No. 1, 1998, pp. 148–155, 10.2514/2.4211.

[8] Z. Dang, "New State Transition Matrix for Relative Motion on an Arbitrary Keplerian Orbit," *Journal of Guidance, Control, and Dynamics*, Vol. 40, No. 11, 2017, pp. 2917–2927, 10.2514/1.G002723.

[9] R. G. Reynolds, "Direct Solution of the Keplerian State Transition Matrix," *Journal of Guidance, Control, and Dynamics*, Vol. 45, No. 6, 2022, pp. 1162–1165, 10.2514/1.G006373.

[10] Z. Dang and H. Zhang, "Linearized relative motion equations through orbital element differences for general Keplerian orbits," *Astrodynamics*, Vol. 2, Sept. 2018, pp. 201–215, 10.1007/s42064-018-0021-1.

[11] S. D. Matthew Willis, Kyle T. Alfriend, "Second-Order Solution for Relative Motion on Eccentric Orbits in Curvilinear Coordinates," *AAS/AIAA Astrodynamics Specialist Conference*, 2019.

[12] R. G. Melton, "Relative Motion Between Hyperbolic Trajectories – A Technical Footnote," *73rd International Astronautical Congress, Paris, France*, 2022.

[13] H. J. Allen and A. J. Eggers, "A Study of the Motion and Aerodynamic Heating of Ballistic Missiles Entering the Earth's Atmosphere at High Supersonic Speeds," Tech. Rep. 1381, NACA, 1958.

[14] S. W. Albert, H. Schaub, and R. D. Braun, "Flight Mechanics Feasibility Assessment for Co-Delivery of Direct-Entry Probe and Aerocapture Orbiter," *AIAA Journal of Spacecraft and Rockets*, Vol. 59, No. 1, 2022, pp. 19–32, https://doi.org/10.2514/1.A34953.

[15] S. W. Albert and H. Schaub, "Co-Delivery of Multiple Small Probes to the Martian Surface," *AIAA SciTech 2022 Forum*, 2022, pp. 1–14, 10.2514/6.2022-1653.

[16] H. F. York, "Multiple-Warhead Missiles," *Scientific American*, Vol. 229, No. 5, 1973, pp. 18–27.

[17] H. Schaub, "Relative Orbit Geometry Through Classical Orbit Element Differences," *AIAA Journal of Guidance, Control, and Dynamics*, Vol. 27, Sept.–Oct. 2004, pp. 839–848, 10.2514/1.12595.

[18] J. Dormand and P. Prince, "A family of embedded Runge-Kutta formulae," *Journal of Computational and Applied Mathematics*, Vol. 6, No. 1, 1980, pp. 19–26, https://doi.org/10.1016/0771-050X(80)90013-3.

[19] P. Virtanen, R. Gommers, T. E. Oliphant, M. Haberland, T. Reddy, D. Cournapeau, E. Burovski, P. Peterson, W. Weckesser, J. Bright, S. J. van der Walt, M. Brett, J. Wilson, K. J. Millman, N. Mayorov, A. R. J. Nelson, E. Jones, R. Kern, E. Larson, C. J. Carey, İ. Polat, Y. Feng, E. W. Moore, J. VanderPlas, D. Laxalde, J. Perktold, R. Cimrman, I. Henriksen, E. A. Quintero, C. R. Harris, A. M. Archibald, A. H. Ribeiro, F. Pedregosa, P. van Mulbregt, and SciPy 1.0 Contributors, "SciPy 1.0: Fundamental Algorithms for Scientific Computing in Python," *Nature Methods*, Vol. 17, 2020, pp. 261–272, 10.1038/s41592-019-0686-2.

[20] D. A. Vallado, *Fundamentals of Astrodynamics and Applications*, ch. Appendix D, pp. 1041–1042. Microcosm Press, 4th ed., 2013.

[21] H. J. Allen and A. J. Eggers, "A Study of the Motion and Aerodynamics Heating of Missiles Entering the Earth's Atmosphere at High Supersonic Speeds," Tech. Rep. RM A53D28, NASA, 1953.

[22] J. D. Anderson, *Hypersonic and High Temperature Gas Dynamics*. AIAA, 2000.

[23] S. J. Citron and T. C. Meir, "An analytic solution for entry into planetary atmospheres," *AIAA Journal*, Vol. 3, No. 3, 1965, pp. 470–475, 10.2514/3.2888.

[24] Z. R. Putnam and R. D. Braun, "Extension and Enhancement of the Allen–Eggers Analytical Ballistic Entry Trajectory Solution," *Journal of Guidance, Control, and Dynamics*, Vol. 38, Mar. 2015, pp. 414–430, 10.2514/1.G000846.

[25] P. N. Desai and G. D. Qualls, "Stardust Entry Reconstruction," *Journal of Spacecraft and Rockets*, Vol. 47, No. 5, 2010, pp. 736–740, 10.2514/1.37679.

[26] D. A. Kontinos and M. J. Wright, "Introduction: Atmospheric Entry of the Stardust Sample Return Capsule," *Journal of Spacecraft and Rockets*, Vol. 47, No. 6, 2010, pp. 865–867, 10.2514/1.52887.

[27] H. H. King, "Ballistic missile re-entry dispersion," *Journal of Spacecraft and Rockets*, Vol. 17, No. 3, 1980, pp. 240–247, 10.2514/3.28031.

[28] B. Fegley Jr., *Properties and Composition of the Terrestrial Oceans and of the Atmospheres of the Earth and Other Planets*, pp. 320–345. American Geophysical Union (AGU), 1995, https://doi.org/10.1029/RF001p0320.

[29] F. Leslie and C. Justus, "The NASA Marshall Space Flight Center Earth Global Reference Atmospheric Model—2010 Version," Tech. Rep. NASA/TM—2011–216467, NASA, 2011.